Graphene nanoribbons exfoliated from graphite surface dislocation bands by electrostatic force

2010 Nanotechnology 21 195704

(http://iopscience.iop.org/0957-4484/21/19/195704)

Nanotechnology **21** (2010) 195704 (5pp) doi:10.1088/0957-4484/21/19/195704

Graphene nanoribbons exfoliated from graphite surface dislocation bands by electrostatic force

Anton N Sidorov[1,2,3], **Tanesh Bansal**[2], **P J Ouseph**[1] **and Gamini Sumanasekera**[1,4]

[1] Department of Physics, University of Louisville, Louisville, KY 40292, USA
[2] Department of Electrical and Computer Engineering, University of Louisville, KY 40208, USA
[3] Department of Physics, Georgia Institute of Technology, Atlanta, GA 30332, USA

E-mail: gusuma01@louisville.edu

Received 9 December 2009, in final form 29 March 2010
Published 21 April 2010
Online at stacks.iop.org/Nano/21/195704

Abstract

We have developed a novel technique to produce long and narrow graphene ribbons with smooth edges. This technique is free of any chemical treatments and involves a combination of two steps: (i) creation of surface dislocation ribbons by high velocity clusters impacting the graphite surface and (ii) electrostatic transferring of the dislocation ribbons to a desired substrate. The width of the ribbons can be controlled by varying the impact velocity of a cluster jet stream from a gas jet impactor. The electrical transport properties were investigated on the ribbons in field effect transistor (FET) configuration. The p-type behavior observed under ambient conditions was found to be reversed upon annealing at 180 °C in a vacuum of 10^{-7} Torr. Charge transfer effects were observed when the degassed graphene was exposed to N_2O and NH_3.

(Some figures in this article are in colour only in the electronic version)

Recently graphene consisting of a monolayer to few layers has been extensively studied not only for its interesting physical and chemical properties, but also as a potential material for future electronic devices [1]. Graphene shows intriguing transport properties such as high carrier mobility, room temperature quantum Hall effect, ballistic transport, etc [2, 3]. Two-dimensional graphene is a semi-metal with a zero band and not suitable for transistor applications. Graphene nanoribbons with small enough width to impose lateral confinement effects are predicted to open up a band gap making them a semiconductor. Lithographical patterning of large graphene layers allows one to create graphene ribbons [4] with rough edges. Recently a chemical route has been developed to produce graphene nanoribbons with width smaller than 10 nm exhibiting semiconducting properties. Here we report a new method which does not require any chemical treatments to produce extra long graphene nanoribbons. In a previous paper we have shown that small graphene sheets, often found on cleaved graphite surfaces, can be removed from graphite and can be deposited on to a desired substrate by applying an electrostatic force [5]. One possible drawback of this method is that the graphene sheets thus obtained are irregular in shape. Liang *et al* recently used a lithographic technique in conjunction with electrostatic force to obtain narrow ribbons. Smoothness of the edges in this technique still remains a problem. In this paper we report a new and simple method of producing narrow ribbons of graphene by electrostatically transferring graphite surface dislocation ribbons produced by high velocity clusters impacting graphite surface. Several types of graphite dislocations and defects produced by cluster impact and by cellophane tape cleaving have been discussed in the literature [6–10]. High velocity cluster impact is more reliable than mechanical cleaving in producing dislocation bands and therefore is utilized in the studies reported here. The graphene ribbons obtained by this technique are narrow, long, and consist of smooth edges. Graphene nanoribbon based field effect transistor (FET) characteristics were studied under ambient conditions, degassed conditions, and upon exposure to donor and acceptor gases.

[4] Author to whom any correspondence should be addressed.

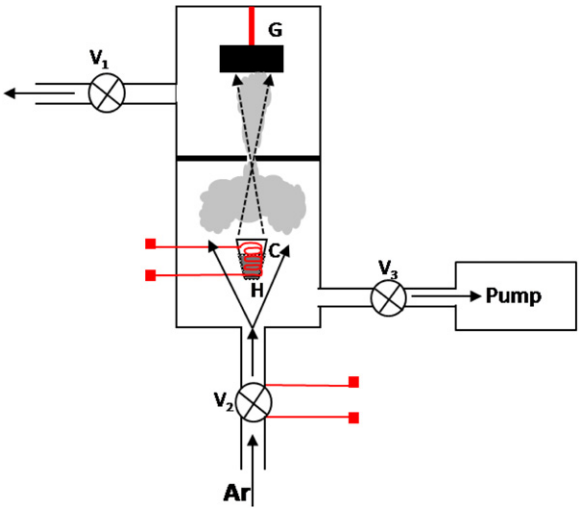

Figure 1. The schematics of the gas jet impactor. Metal clusters reaching graphite through the orifice impact the graphite surface and produce different forms of surface distortions including dislocation lines and nano-craters.

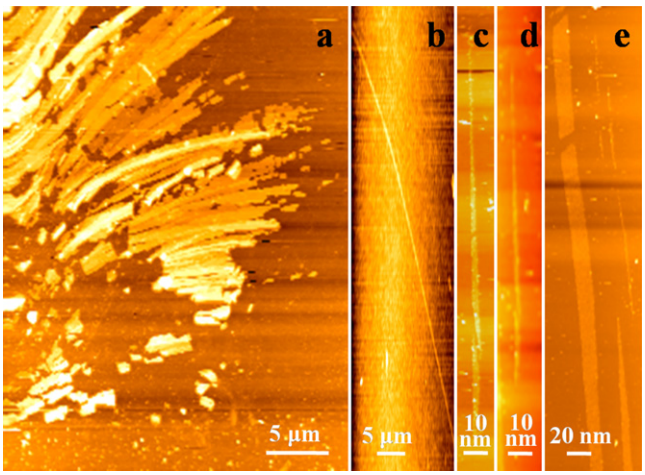

Figure 2. AFM images of the graphene ribbons produced by cluster collision. (a) A dense region of dislocation ribbons directed radially around the center of the collision region. (b)–(e) Long individual graphene nano-ribbons (GNRs) transferred to the Si/SiO_2 substrate.

The novel technique that was developed in our laboratory uses a gas jet impactor [11] for producing dislocation ribbons on the graphite surface. We begin by cleaving a highly oriented graphene (HOPG) surface with Scotch tape. Then, the cleaved graphite (G) is placed in the upper half of the chamber with the cleaved surface facing down, as shown in figure 1. A low melting point metal such as indium or gallium is placed in crucible (C) in the bottom half of the chamber. The crucible is surrounded by a resistive heater (H). Both parts of the chamber are connected to each other through an orifice approximately 0.5 mm in diameter. The gas impactor consists of three valves V_1, V_2, and V_3. The top half of the chamber is connected to the atmosphere through valve V_1 and can be used to release high pressure build up. An electromagnetic actuator, V_2, is connected to the bottom half of the chamber and allows bursts of high pressure argon gas into the chamber when needed. The valve, V_2 opens instantaneously when a voltage is applied to the actuator and remains open as long as the voltage is on. The valve, V_3 connects the bottom half of the chamber to the mechanical pump which evacuates air from the chamber.

First, the valves V_2 and V_1 remain closed and the valve V_3 is opened to allow evacuation of the two chambers. When the pressure reaches a desired value, the valve V_3 is closed and the necessary electric current is allowed to flow through the heater coil surrounding the crucible. The piece of metal (indium) in the crucible attains boiling temperature and creates a cloud of metal clusters around the crucible, as shown in figure 1. By applying a voltage to the actuator, the pneumatic valve, V_2, is opened instantaneously, allowing a burst of high pressure argon gas into the bottom half of the chamber. The gas jet through the orifice carries metal clusters with it into the top chamber. The speed of the clusters carried by the gas jet depends on the argon gas pressure and therefore can be adjusted by changing the pressure of the gas. Experimentally determined speed of the clusters is found to be in the range of 10–50 m s^{-1} in our experiments.

Metal clusters reaching graphite through the orifice impact the graphite surface and produce different forms of surface distortions including dislocation ribbons and nano-craters. The clusters impacting the graphite surface at an angle larger than 90° with respect to the surface are found to produce dislocation bands. The horizontal components of the momentum of the incoming clusters cause sliding of sections of graphene along its direction producing ribbons. Therefore, dislocation ribbons are observed to radiate radially from the center of the region of impact. The production of dislocation ribbons is a consequence of the weaker binding between graphite layers in comparison to strong covalent bonding between sp^2 carbon atoms. Therefore, it can be concluded that the length and width of the ribbons depend on the magnitude of the energy transferred to the graphite surface by the clusters, which in turn depends on the velocity of the gas jet and the mass of the metal (gallium, mercury, etc). Figure 2(a) is an atomic force microscopy (AFM) picture of ribbons radiating from the center of the cluster collision region located close to the bottom left-hand corner of the picture. The steps followed to obtain ribbons in figure 2(a) are: (i) the graphite surface is first cleaved to obtain a smooth surface; (ii) the graphite sample is then placed in the top part of the chamber with the clean surface facing the orifice; (iii) the argon gas with clusters is allowed to bombard the graphite surface.

The electrostatic deposition (ESD) technique is found to be suitable to transfer graphene dislocation ribbons onto a variety of substrates. Figures 2(b)–(e) show AFM pictures of ribbons electrostatically transferred on to the Si/SiO_2 substrate. The electrostatic field is produced by applying 50 V across two electrodes separated by ∼0.5 mm. Graphite with dislocations is attached to one of the electrodes and the substrate to the other.

At this point two important questions need to be answered. (i) Why does the electric field only transfer dislocation ribbons? (ii) Are the edges of the ribbons jagged or smooth? Answers to both questions may be obtained from the scanning

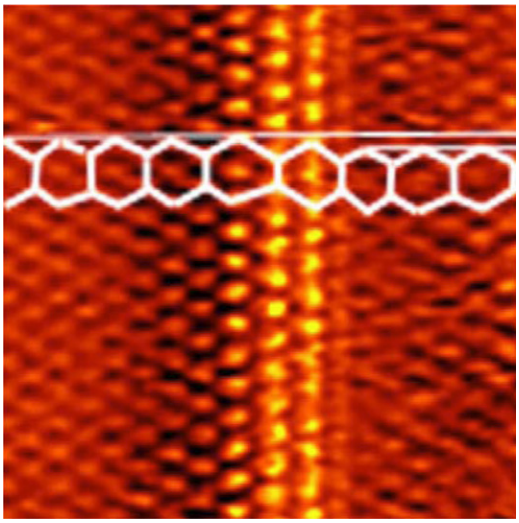

Figure 3. STM image of a dislocation band.

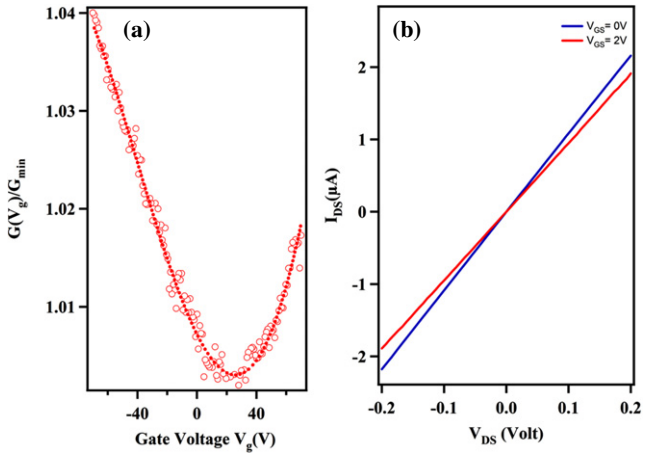

Figure 4. (a) The conductance normalized to the minimum conductance, $G(V_g)/G_{min}$ versus V_g of the monolayer graphene FET under ambient conditions. We found our graphene FET to be p-type with net charge $n_0 > 0$. (b) Drain–source current (I_{DS}) versus the drain–source voltage (V_{DS}) under different gate voltages ($V_g = 0, 2$ V).

tunneling microscopy (STM) studies of dislocation ribbons reported in [6] and [9]. The layers in normal graphite have 'aba' stacking order while the dislocation region in [6] and [9] has 'abb' stacking and 'abc' stacking, respectively. Because of the differences in the stacking order, the average electron density on the surface changes. The average charge density in the regions of 'aba' stacking (normal stacking), 'abc' stacking, and 'abb' stacking has been estimated to be 0.0033, 0.0056, and 0.0085 states/eV spin, respectively. This difference in the charge density increases the force acting on the atoms in the dislocation regions in an electric field compared to the force on the atoms in the surrounding normal regions. Also the binding energy of atoms in 'abc' and 'aaa' stacking have been estimated to be less than the atoms in 'aba' stacking by 0.11 and 9.68 meV/atom, respectively [12]. For these two reasons only dislocation regions are removed from the graphite surface to the substrate provided the electric field is not too strong. Also since the electrostatic force is acting only on the atoms in the dislocation ribbons the transferred ribbons are only one layer thick. Our measurements support this conclusion. Figure 3 shows the STM picture of a dislocation band (reproduced with permission from [9]). This figure clearly shows the smoothness of the edges with single atoms lined up along the boundaries. The transferred ribbons, therefore, should have similar smooth edges.

For electrical characterization, the graphene ribbons (GR) produced on the freshly cleaved HOPG surface by metal cluster impact were transferred onto degenerately doped p-type silicon with a 300 nm thick SiO_2 insulating layer. Then, Au/Ti metal contacts were deposited for FET fabrication employing e-beam lithography with silicon as the back gate. The single layers were identified by their color under an optical microscope and confirmed by Raman spectroscopy and AFM. The graphene FET on Si was then placed in a chip carrier and packaged. The chip carrier was mounted onto a socket supported in the base of a probe contained within a stainless steel tube (0.75 cm diameter × 30 cm long) that was connected to a gas manifold and turbo-molecular vacuum pump. The tube was inserted into a tube furnace and could be evacuated to 2×10^{-7} Torr. A type-K thermocouple was mounted on the chip carrier near the Si substrate to monitor the local temperature. The measurements involved monitoring of the source–drain current (I_{DS}) as a function of the gate voltage (V_g) for a given source–drain voltage (V_{DS}) under various environments.

The experiment was first conducted under ambient conditions in air at room temperature and atmospheric pressure. We observed the Dirac point in G_{DS} at positive V_g (i.e. $+20$ V $< V_g < +30$ V) as shown in figure 4(a). The dotted line is a guide to the eye. Figure 4(b) shows I_{DS} versus the V_{DS} for two different gate voltages ($V_g = 0, 2$ V).

From the measured I–V characteristics in the linear region, the carrier (hole and electron) mobilities can be deduced by using

$$\mu = \frac{\Delta I_{DS}}{C_{ox} \frac{w}{L} V_{DS} \Delta V_g}. \quad (1)$$

where μ is the carrier mobility, W and L are FET width and length, respectively, $C_{ox} = \varepsilon_{ox}\varepsilon_0/t_{ox}$ is the gate oxide capacitance ($\varepsilon_{ox} = 3.9$ is silicon dioxide permittivity and $t_{ox} = 300$ nm is the gate oxide thickness), and ΔI_{DS} is induced by ΔV_g.

The I–V characteristics of a FET with a graphene thickness of $d = 0.46$ nm, a gate oxide thickness of $t_{ox} = 300$ nm, a graphene channel width of $W = 53$ nm, and a channel length of $L = 6.1$ μm are shown in figure 4. The linear I_{DS} versus V_{DS} behavior (figure 4(b)) indicates a good ohmic contact between Ti/Au contact pads and graphene channels. The G versus V_g curve (figure 4(a)) shows that the gate can influence either hole or electron conduction. The G minimum occurs at $V_g \sim 21$ V. A gate oxide capacitance is found to be $C_{ox} = 1.17 \times 10^{-4}$ F m^{-2} for our samples. Therefore, using the FET parameters given above, the field effect mobilities are $\mu_h = 4483$ cm^2 V^{-1} s^{-1} and $\mu_e = 3905$ cm^2 V^{-1} s^{-1},

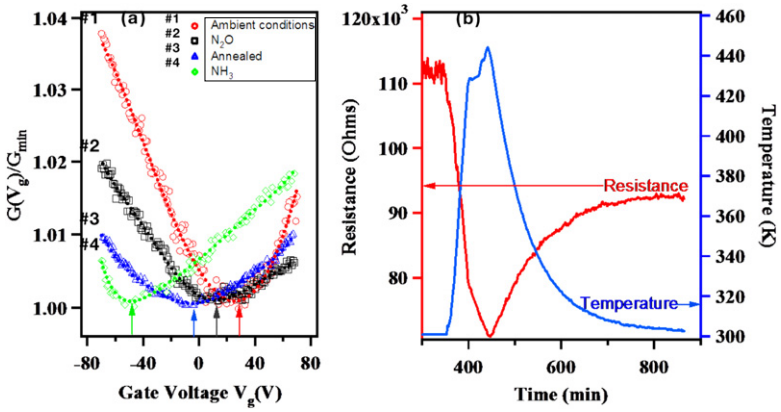

Figure 5. (a) Gate voltage dependence of conductivity caused by graphene under ambient conditions (red #1), after vacuum annealing at ∼180 °C at ∼2 × 10^{-7} Torr (blue #3), upon exposure to 1 atm ammonia (green #4) and nitrous oxide (black #2). V_{DS} = 200 mV. (b) The time evaluation of the source–drain resistance and corresponding temperature during the vacuum annealing process at V_g = 0 V.

respectively. The mobilities are among the values previously reported [13–15]. The hole mobility in our devices is higher than the electron mobility, which is consistent with previous work in graphene FETs fabricated by mechanical exfoliation and epitaxial growth [13–15]. This asymmetry in carrier mobilities, contradicting the prediction based on the symmetry of ideal graphene's conduction and valence bands, is attributed to the extrinsic doping from the substrate [16, 17].

We found that the observed p-doping under ambient conditions could be reversed to n-doping by vacuum annealing at ∼180 °C at ∼10^{-7} Torr as shown in figure 5. Figure 5(b) shows the temperature dependence of the resistance during the degassing at 180 °C in a vacuum of 10^{-7} Torr. As can be seen, the resistance decreases during the degassing. Further, the Dirac point was found to downshift during the degassing. When the Dirac point reached almost the neutrality point, the temperature was brought down to room temperature.

As can be seen from figure 5(a), the Dirac peak shifts to the neutrality point for the annealed sample. Further annealing is expected to bring the Dirac point further into the negative [18]. This n-type behavior can be interpreted as due to the charge transfer from surface states on SiO_2 to graphene. P-type behavior under ambient is believed to be an electrochemically mediated charge transfer from graphene to oxygen [18, 19]. After annealing, the graphene FET was exposed to nitrous oxide. Doping with N_2O not only adds holes to the valence band, but also induces charged impurities. The Dirac peak shifts back to the positive side of V_g and the graphene FET was found to be p-type again. Conductivity, G, of single-layer graphene away from the neutrality point changes approximately linearly with increasing V_g and the steepness of the $G(V_g)$ curves (away from the neutrality point) characterizes the mobility, μ.

The charge carrier mobilities in the annealed graphene are estimated to be μ_h = 2147 $cm^2\,V^{-1}\,s^{-1}$ and μ_e = 2173 $cm^2\,V^{-1}\,s^{-1}$, respectively. Also, a significant broadening of the transition region near the neutrality point is clearly seen on the $G(V_g)$-curves in figure 5. This broadening could in principle be attributed to an increasingly inhomogeneous distribution of dopants [20, 21]. However, such a strong broadening was found to be specific for annealed and N_2O samples. The charge carrier mobilities in the graphene exposed to N_2O are μ_h = 2282 $cm^2\,V^{-1}\,s^{-1}$ and μ_e = 1771 $cm^2\,V^{-1}\,s^{-1}$, respectively. We found that the initial undoped state could be recovered by repeating the annealing process at 180 °C in a vacuum of ∼10^{-7} Torr. Repetitive exposure–annealing cycles showed no 'poisoning' effects of the introduced chemicals (that is, the devices could be annealed back to their initial state). Then, when the device was in the initial undoped state we introduced NH_3 as shown in figure 5(a). In the observed doping process NH_3 acts as an electron donor to graphene. So, n-type behavior of the graphene FET exposed to ammonia was observed and the Dirac peak was shifted to the far left (<−50 V) from the neutrality point. Also the electron branch becomes prominent compared to the hole branch, as expected.

In conclusion, we have successfully developed a novel technique to produce long and narrow graphene ribbons with smooth edges by transferring surface dislocation bands, produced by high velocity clusters impacting a graphite surface, by electrostatic force to a desired substrate. The average width of the GNR is found to be ∼30 nm, but the technique has the promise to generate NRs with considerably smaller widths. The width of the ribbons can be controlled by varying the impact velocity and the direction of the jet stream. The electrical transport properties investigated on the ribbons in FET configuration shows that the observed p-type behavior observed under ambient conditions can be reversed upon annealing at high temperature in a vacuum. This n-type behavior under degassed conditions is attributed as due to the charge transfer from surface states on SiO_2 to graphene. P-type behavior under ambient is believed to be due to electrochemically mediated charge transfer from graphene to oxygen [22]. Charge transfer effects were observed when the degassed graphene was exposed to N_2O and NH_3.

References

[1] Lin Y-M, Jenkins K A, Valdes-Garcia A, Small J P, Farmer D B and Avouris P 2009 Operation of graphene transistors at gigahertz frequencies *Nano Lett.* **9** 422–6

[2] Bolotin K I, Sikes K J, Jiang Z, Klima M, Fudenberg G, Hone J, Kim P and Stormer H L 2008 Ultrahigh electron mobility in suspended graphene *Solid State Commun.* **146** 351–5
[3] K S Novoselov, Jiang Z, Zhang Y, Morozov S V, Stormer H L, Zeitler U, Maan J C, Boebinger G S, Kim P and Geim A K 2007 Room-temperature quantum Hall effect in graphene *Science* **315** 1379
[4] Liang X, Chang A S P, Zhang Y, Harteneck B D, Choo H, Olynick D L and Cabrini S 2009 Electrostatic force assisted exfoliation of prepatterned few-layer graphenes into device sites *Nano Lett.* **9** 919
[5] Sidorov A N, Yazdanpanah M M, Jalilian R, Ouseph P J, Cohn1 R W and Sumanasekera G U 2007 Electrostatic deposition of graphene *Nanotechnology* **18** 135301
[6] Ouseph P J 2000 Scanning tunneling microscopy observation of dislocations with superlattice structure in graphite *Appl. Surf. Sci.* **165** 38–43
[7] Ouseph P J and Poothackanal T 1996 Scanning tunneling microscopy observations of mercury droplets on graphite *Langmuir* **12** 3920–6
[8] Ouseph P J 1996 Transformation of a graphite superlattice into triangular dislocations *Phys. Rev.* B **53** 9610–3
[9] Ouseph P J 2009 Graphite dislocations induced by collision of neutral mercury droplets *Appl. Surf. Sci.* **256** 96–8
[10] Chang H and Bard A J 1991 Observation and characterization by scanning tunneling microscopy of structures generated by cleaving highly oriented pyrolytic graphite *Langmuir* **7** 1143–53
[11] Cambel A B and Jennings B H 1958 *Gas Dynamics* (New York: McGraw-Hill)
[12] Telling R H and Heggie M I 2003 Stacking fault and dislocation glide on the basal plane of graphite *Phil. Mag. Lett.* **83** 411–21
[13] Lemme M C, Echtermeyer T J, Baus M and Kurz H 2007 *IEEE Electron Device Lett.* **28** 282–4
[14] Gu G, Nie S, Feenstra R M, Devaty R P, Choyke W J, Chan W K and Kane M G 2007 *Appl. Phys. Lett.* **90** 253507
[15] Inokawa H, Nagase M, Hirono S, Goto T, Yamaguchi H and Torimitsu K 2007 *Japan. J. Appl. Phys.* 1 **46** 2615–7
[16] Chen Z, Lin Y-M, Rooks M J and Avouris P 2007 Graphene nano-ribbons electronics *Physica* E **40** 228–32
[17] Romero H E, Shen Ning, Joshi P, Gutierrez H R, Tadigadapa S A, Sofo J O and Eklund P C 2008 n-type behavior of graphene supported on Si/SiO_2 substrates *ACS Nano* **2** 2037–44
[18] Novoselov K S, Geim A K, Morozov S V, Jiang D, Zhang Y, Dubonos S V, Grigorieva I V and Firsov A A 2004 Electric field effect in atomically thin carbon films *Science* **306** 666–9
[19] Tan Y W, Zhang Y, Bolotin K, Zhao Y, Adam S, Hwang E H, Das Sarma S, Stormer H L and Kim P 2007 Measurement of scattering rate and minimum conductivity in graphene *Phys. Rev. Lett.* **99** 246803
[20] Geim A K and Novoselov K S 2007 The rise of graphene *Nat. Mater.* **6** 183–91
[21] Hwang E H, Adam S and Das Sarma S 2007 Carrier transport in two-dimensional graphene layers *Phys. Rev. Lett.* **98** 186806
[22] Tchernatinsky A, Desai S, Sumanasekera G U, Jayanthi C S and Wu S Y 2006 Adsorption of oxygen molecules on individual single-wall carbon nanotubes *J. Appl. Phys.* **99** 034306